



CHORUS

This is the accepted manuscript made available via CHORUS. The article has been published as:

Local temperatures of strongly-correlated quantum dots out of equilibrium

LvZhou Ye, Dong Hou, Xiao Zheng, Yijing Yan, and Massimiliano Di Ventra

Phys. Rev. B **91**, 205106 — Published 7 May 2015

DOI: [10.1103/PhysRevB.91.205106](https://doi.org/10.1103/PhysRevB.91.205106)

Local temperatures of strongly-correlated quantum dots out of equilibrium

LvZhou Ye,¹ Dong Hou,¹ Xiao Zheng,^{1,2,*} YiJing Yan,^{1,3,4} and Massimiliano Di Ventra^{5,†}

¹Hefei National Laboratory for Physical Sciences at the Microscale,
University of Science and Technology of China, Hefei, Anhui 230026, China
²Synergetic Innovation Center of Quantum Information and Quantum Physics,
University of Science and Technology of China, Hefei, Anhui 230026, China

³Collaborative Innovation Center of Chemistry for Energy Materials,
University of Science and Technology of China, Hefei, Anhui 230026, China

⁴Department of Chemistry, Hong Kong University of Science and Technology, Clear Water Bay, Hong Kong, China

⁵Department of Physics, University of California, San Diego, La Jolla, California 92093

(Dated: Submitted on March 16, 2015; resubmitted on April 22, 2015)

Probes that measure the local thermal properties of systems out of equilibrium are emerging as new tools in the study of nanoscale systems. One can then measure the temperature of a probe that is weakly coupled to a bias-driven system. By tuning the probe temperature so that the expectation value of some observable of the system is minimally perturbed, one obtains a parameter that measures its degree of local statistical excitation, and hence its local heating. However, one anticipates that different observables may lead to different temperatures and thus different local heating expectations. We propose an experimentally realizable protocol to measure such local temperatures and apply it to bias-driven quantum dots. By means of a highly accurate open quantum system approach, we show theoretically that the measured temperature is quite insensitive both to the choice of observable and to the probe-system coupling. In particular, even with observables that are distinct both physically and in their degree of locality, such as the *local* magnetic susceptibility of the quantum dot and the *global* spin-polarized current measured at the leads, the resulting local temperatures are quantitatively similar for quantum dots ranging from noninteracting to Kondo-correlated regimes, and are close to those obtained with the traditional “local equilibrium” definition.

PACS numbers: 72.20.Pa, 79.10.-n, 71.27.+a, 73.63.Kv

I. INTRODUCTION

Temperature is a thermodynamic quantity of fundamental importance in the description of systems at equilibrium. However, the extension of this concept to systems far from equilibrium is not obvious. From an operational point of view, temperature is defined as that quantity measured by a thermometer coupled to the system with which it reaches thermal equilibrium. Precisely because the thermometer plus the system reach a state of global equilibrium when coupled, the quantity that is measured by the thermometer is then attributed to the system in the limit of weak coupling and negligible heat capacity of the thermometer. This definition is no longer valid for a system out of equilibrium such as one driven by a constant bias¹. In this case, electron-electron interactions and electron-phonon interactions are expected to induce electronic and ionic “temperatures” different from those of the same system at equilibrium¹. The question then is: What are these temperatures and how do we measure them *directly*?

Several solutions have been proposed. For instance, Engquist and Anderson have introduced the concept of ideal potentiometer/thermometer². In this case, local chemical potential and local temperature are defined by a “local equilibrium condition”: the net particle and heat current flowing through the potentiometer/thermometer are set to zero^{3–11}. Although such a definition is appealingly intuitive and has been used extensively in the past, *we do not have means to directly measure heat cur-*

rents (unlike particle currents for which ammeters are available)¹², and therefore its experimental realization is very limited. Other theoretical definitions include the use of approximate distribution functions¹³, information compressibility¹⁴, or generalized fluctuation-dissipation theorems¹⁵, to name just a few (for a more complete set of definitions see, e.g., Ref. 12). All of these, however, suffer from some limitations in their experimental realizations and therefore are also of limited use.

On the experimental side, methods have been devised to determine local temperatures by monitoring properties that are sensitive to thermal fluctuations, such as the bond rupture force¹⁶, the junction lifetime^{17,18}, the mechanical stretching distance¹⁹, the bias-driven current noise²⁰, and the surface-enhanced Raman intensities^{21,22}. These probes, however, provide only an *indirect* measurement of a “local temperature” leaving the original question still open.

There is, instead, an increasing body of experimental studies in which thermal probes are coupled *directly* to driven nanoscale systems with a resolution that is approaching hundreds of nanometers or less^{23–30}, thus making them ideal as *local thermometers*. With these thermometers an operational definition of temperature has been proposed by imposing a *minimal perturbation condition*³¹, in which the temperature of the probe, T_p , is varied, while monitoring some observable of the system, in such a way that the expectation value of that observable is minimally perturbed. The probe temperature satisfying this condition is then a parameter attributed to

the system, which characterizes its local excitations out of equilibrium. This type of definition has been used, for instance, in the study of the thermoelectric response of nanoscale systems to applied thermal gradients, leading to the prediction of temperature oscillations^{10,32}. It is an operational definition that is relatively straightforward to implement experimentally. However, it leaves open the prescription of what type of observable one should use, and whether different observables lead to quantitatively different temperatures. In addition, in the original paper³¹, the thermal probe was assumed to be a bosonic system, and hence no electric current could flow between the system and the probe. This is quite a strong limitation since the experimental probes that are being developed are generally fermionic systems^{23–30}. In this case, an extra constraint related to the local chemical potential of the thermal probe needs to be introduced.

In this paper, we discuss a protocol to measure the local temperature of a system out of equilibrium that is coupled to a thermal probe. We consider a fermionic probe and allow the measurement of an observable of the system in such a way that the minimal perturbation condition be satisfied. We show that by appropriately setting the chemical potential of the probe at the beginning of the measurement, the choice of observables quite distinct both physically and in their degree of locality lead to local temperatures that are quantitatively similar even for strongly correlated systems, and very close to those obtained with the often-used local equilibrium temperature. These results lend support to the extrapolated parameter as the “temperature” of the system.

The remainder of this paper is organized as follows. In Sec. II we propose an experimentally realizable protocol to measure local temperatures for quantum dot (QD) systems out of equilibrium. We then give a brief introduction on the basic features of the hierarchical equations of motion approach, which is used to carry out the numerical investigations in this paper. In Sec. III we demonstrate the usefulness and practicality of the proposed operational protocol by applying it to QDs in both noninteracting and Kondo-correlated regimes. Finally, concluding remarks are given in Sec. IV.

II. METHODOLOGY AND MODEL

A. An operational protocol for the determination of local temperature

We consider a quantum dot in contact with two leads as sketched in Fig. 1. Under a bias voltage or a thermal gradient across the two leads, the temperatures (chemical potentials) of left and right leads are T_L and T_R (μ_L and μ_R), respectively. To determine the local temperature T^* and local chemical potential μ^* of the QD, the dot is coupled to a third lead (the probe), whose chemical potential μ_p and temperature T_p are tunable.

The first step of the protocol we suggest is the deter-

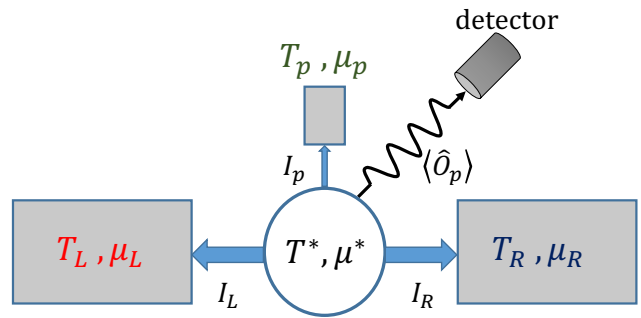


FIG. 1. Schematic diagram of the proposed protocol for the measurement of local temperature in a QD connected to two leads (L and R). A weakly coupled probe with tunable μ_p and T_p is used. The expectation value of an observable, O_p , is monitored while T_p is varied.

mination of the chemical potential of the probe. Ideally, at zero bias (equilibrium) the minimal perturbation condition³¹ should yield exactly the background equilibrium temperature T_{eq} . This can be accomplished as follows. In the presence of an applied bias voltage or a thermal gradient³³, we first determine μ^* as

$$\mu^* = \zeta_L \mu_L + \zeta_R \mu_R. \quad (1)$$

The weight coefficients ζ_L and ζ_R are determined by³⁴

$$\zeta_\alpha = 1 - \left| \frac{I_p(T_\alpha, \mu_\alpha)}{I_p(T_L, \mu_L) - I_p(T_R, \mu_R)} \right|. \quad (2)$$

Here, $I_p(T_\alpha, \mu_\alpha)$ is the electric current measured at the probe, by setting the chemical potential and temperature of the probe to be identical with those of lead- α .

We then set $\mu_p = \mu^*$, and monitor the change of a given system observable $O = \langle \hat{O} \rangle$ as T_p varies. The local temperature T^* is finally determined by the minimal perturbation condition³¹

$$T^* = \arg \min_{T_p} |O_0 + \delta O_p - O_p(T_p, \mu^*)|. \quad (3)$$

Here, O_0 is the expectation value of \hat{O} measured without the probe, while $O_p(T_p, \mu^*)$ is its measured value with the probe coupled to the dot. The nonzero probe-dot coupling, Δ_p , results in a finite perturbation to the intrinsic dot properties. This effect is accounted for by the correction term δO_p in Eq. (3) determined by

$$\delta O_p = \zeta_L O_p(T_L, \mu_L) + \zeta_R O_p(T_R, \mu_R) - O_0. \quad (4)$$

Here, $O_p(T_\alpha, \mu_\alpha)$ is measured by setting T_p and μ_p to be identical to their counterparts of lead- α . In doing so, the probe is deemed as part of lead- α . Since the QD is coupled to both left and right leads, the overall influence of the probe can be estimated as a weighted average given by Eq. (4). There, the weight coefficients $\{\zeta_\alpha\}$ are assumed to be same as those used in Eq. (1).

Note that the protocol proposed above is easily realizable experimentally, and is universally applicable to any QD system. Also, for all the QDs studied in this work, the minimal perturbation of $\langle \hat{O} \rangle$ searched for in Eq. (3) is always found to be zero, *i.e.*, $O_p(T_p, \mu^*) = O_0 + \delta O_p$ can always be satisfied at a certain T_p . This indicates that the chosen observable O_p changes monotonically and sensitively as T_p varies in the vicinity of T^* .

It is important to verify that at exactly zero bias the local temperature measured by the minimal perturbation condition is exactly the physical equilibrium temperature T_{eq} . This can be seen from Eqs. (1)–(4). At zero bias, we find that from Eq. (1) the local chemical potential is just the equilibrium Fermi energy. Then Eq. (3) reduces to the simple form $O_p(T_p) = O_p(T_{\text{eq}})$, with the trivial solution $T_p = T_{\text{eq}}$.

B. Hierarchical equations of motion approach for quantum impurity systems

We now apply Eqs. (1)–(4) to QD systems described by a single-impurity Anderson model (SIAM)^{35,36}. The total Hamiltonian of the QD system is $H = H_{\text{dot}} + H_{\text{lead}} + H_{\text{coupling}}$. The dot is described by $H_{\text{dot}} = \epsilon_d \hat{n}_d + U \hat{n}_\uparrow \hat{n}_\downarrow$. Here, $\hat{n}_d = \sum_s \hat{n}_s = \sum_s \hat{a}_s^\dagger \hat{a}_s$, where \hat{a}_s^\dagger (\hat{a}_s) creates (annihilates) a spin- s electron on the dot energy level ϵ_d , and U is the on-dot electron-electron interaction strength. $H_{\text{lead}} = \sum_{\alpha k s} \epsilon_{\alpha k} \hat{d}_{\alpha k s}^\dagger \hat{d}_{\alpha k s}$ and $H_{\text{coupling}} = \sum_{\alpha k s} t_{\alpha k} \hat{a}_s^\dagger \hat{d}_{\alpha k s} + \text{H.c.}$ represent the noninteracting leads and dot-lead couplings, respectively. Here, $\hat{d}_{\alpha k s}^\dagger$ ($\hat{d}_{\alpha k s}$) creates (annihilates) an electron on the orbital $|k\rangle$ of lead- α ($\alpha = L, R$ or p); and $t_{\alpha k}$ is the coupling strength between the dot level and lead orbital $|k\rangle$.

We employ a hierarchical equations of motion (HEOM) approach to compute the reduced density matrix ρ of open fermionic systems^{37,38}, so as to characterize the equilibrium and nonequilibrium properties of the SIAM^{39,40}. The HEOM approach has been used to study static and dynamic Kondo effects in QDs^{41–45}, and it is in principle exact if all orders of the hierarchy expansion were included. In practice, the numerical results converge to the exact values rapidly and uniformly with the increasing truncation level of the hierarchy. Once the convergence is achieved, the results are guaranteed to be quantitatively accurate³⁸.

The derivation of the HEOM formalism for fermionic environment has been detailed in Refs. 37, 41, 43, and 46. Here, we only introduce some of its basic features. The final form of the HEOM can be cast into a compact form as follows³⁷

$$\begin{aligned} \dot{\rho}_{j_1 \dots j_n}^{(n)} = & - \left(i\mathcal{L} + \sum_{r=1}^n \gamma_{j_r} \right) \rho_{j_1 \dots j_n}^{(n)} - i \sum_j \mathcal{A}_j \rho_{j_1 \dots j_n j}^{(n+1)} \\ & - i \sum_{r=1}^n (-)^{n-r} \mathcal{C}_{j_r} \rho_{j_1 \dots j_{r-1} j_{r+1} \dots j_n}^{(n-1)}. \end{aligned} \quad (5)$$

Here, $\rho^{(0)}(t) = \rho(t) \equiv \text{tr}_{\text{env}} \rho_{\text{total}}(t)$ is the reduced density matrix, and $\{\rho_{j_1 \dots j_n}^{(n)}(t); n = 1, \dots, L\}$ are the auxiliary density matrices, with L denoting the truncation level. Usually a relatively low L (say, $L = 4$ or 5) is often sufficient to yield quantitatively converged results.

In Eq. (5) the multi-component index $j \equiv (\sigma \alpha \mu \nu m)$ characterizes the transfer of an electron from/to ($\sigma = +/-$) the impurity level- μ to/from level- ν via the α th lead and associated with a characteristic memory time γ_m^{-1} . The Grassmann superoperators $\mathcal{A}_j \equiv \mathcal{A}_{\mu}^{\bar{\sigma}}$ and $\mathcal{C}_j \equiv \mathcal{C}_{\mu \nu m}^{\sigma}$ are defined via their fermionic/bosonic actions on an operator \hat{O} as $\mathcal{A}_{\mu}^{\bar{\sigma}} \hat{O} \equiv [\hat{a}_{\mu}^{\bar{\sigma}}, \hat{O}]_{\mp}$ and $\mathcal{C}_{\mu \nu m}^{\sigma} \hat{O} \equiv \eta_{\mu \nu m}^{\sigma} \hat{a}_{\nu}^{\bar{\sigma}} \hat{O} \pm (\eta_{\mu \nu m}^{\bar{\sigma}})^* \hat{O} \hat{a}_{\nu}^{\sigma}$, respectively, with $\bar{\sigma}$ being the opposite sign of σ . The on-dot electron interactions are contained in the Liouvillian of impurities, $\mathcal{L} \cdot \equiv [H_{\text{dot}}, \cdot]$.

In the framework of the HEOM, the effect of the leads is captured by the hybridization functions $\Delta_{\alpha}(\omega) \equiv \pi \sum_k |t_{\alpha k}|^2 \delta(\omega - \epsilon_{\alpha k})$. For numerical convenience, a Lorentzian form $\Delta_{\alpha}(\omega) = \Delta_{\alpha} W^2 / [(\omega - \mu_{\alpha})^2 + W^2]$ is adopted, where Δ_{α} is the coupling strength between the dot and lead- α , and W is the lead band width. Hereafter, $\Delta = \Delta_L + \Delta_R$ is taken as the unit of energy.

The expectation value of any system observable \hat{O} is computed via $O = \text{tr}(\rho \hat{O})$. The energy distribution of electric and heat currents flowing into lead- α as required to determine T^* with the “local equilibrium condition”^{47–50} are calculated as

$$\begin{aligned} j_{\alpha}^k(\omega) = & (-1)^{k+1} \left(\frac{i}{\pi} \right) (\omega - \mu_{\alpha})^k \Delta_{\alpha}(\omega) \\ & \times \{ \mathcal{G}^<(\omega) + 2i f_{\beta}(\omega - \mu_{\alpha}) \text{Im}[\mathcal{G}^r(\omega)] \}. \end{aligned} \quad (6)$$

Here, we have set $e = \hbar = 1$; $k = 0$ and 1 correspond to the electric and heat currents, respectively; $f_{\beta}(\omega)$ is the Fermi function; and the lesser and retarded Green’s functions $\mathcal{G}^<$ and \mathcal{G}^r are computed from correlation functions. The global electric and heat currents flowing into lead- α are $I_{\alpha} = \int d\omega j_{\alpha}^0(\omega)$ and $J_{\alpha}^H = \int d\omega j_{\alpha}^1(\omega)$, respectively. Note that the electron-phonon interactions and the phonon contribution to heat current have been neglected, since their effects are negligibly small in QDs at low temperatures⁵¹.

To have an accurate measurement of T^* and thus test its robustness with respect to the choice of observables, the probed observable O must vary sensitively with T_p . We then choose some spin-related properties, because spin polarization processes require low excitation energies. A promising candidate is the *local* magnetic susceptibility

$$\chi^m(\omega) = i \int_0^{\infty} dt e^{i\omega t} \langle [\hat{m}_z(t), \hat{m}_z(0)] \rangle. \quad (7)$$

Here, $\hat{m}_z = g\mu_B(\hat{n}_{\uparrow} - \hat{n}_{\downarrow})/2$ is the local magnetic moment due to on-dot spin polarization, g is the gyromagnetic ratio and μ_B is the Bohr magneton. In this work, we focus only on the zero-frequency (static) component of $\chi^m(\omega)$, *i.e.*, $\chi^m \equiv \chi^m(\omega = 0) = i \int_0^t dt \langle [\hat{m}_z(t), \hat{m}_z(0)] \rangle =$

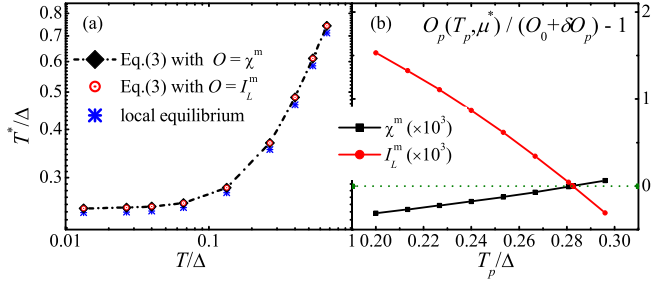


FIG. 2. (a) Local temperature T^* of a noninteracting QD determined by different protocols versus background T . The dashed line is a guide to eyes. (b) Variation of the local magnetic susceptibility χ^m and total spin current I_L^m with T_p at a background $T = 0.133\Delta$. The parameters adopted are (in units of Δ): $\epsilon_d = -2.67$, $U = 0$, $\Delta_L = 2\Delta_R = 0.67$, $\mu_R = -\mu_L = 0.53$, and $W = 40$.

$\lim_{H_z \rightarrow 0} \langle \hat{n}_z \rangle / H_z$, with H_z being the applied magnetic field. It has been demonstrated that the HEOM approach is capable of yielding highly accurate χ^m for strongly correlated QDs; see Fig. 4 of Ref. 40. Another choice is the *global* spin-polarized current

$$I_\alpha^m = \langle \hat{I}_{\alpha\uparrow} \rangle - \langle \hat{I}_{\alpha\downarrow} \rangle, \quad (8)$$

with $\hat{I}_{\alpha s} = i \sum_k [\hat{n}_{\alpha ks}, H_{\text{coupling}}]$. The different degree of locality of these quantities provides an even stronger test for our operational protocol.

III. RESULTS AND DISCUSSIONS

A. Local temperature of a noninteracting QD

We consider first a noninteracting QD ($U = 0$) under a bias voltage $\mu_R = -\mu_L = \frac{1}{2}V$. The HEOM method has the virtue that, for noninteracting systems the hierarchy terminates automatically at $L = 2$ without any approximation³⁷. Figure 2(a) plots T^* determined by Eqs.(1)–(4) versus the background temperature $T = T_L = T_R$. We have set the dot-lead couplings to be asymmetric with $\Delta_L = 2\Delta_R$. The weight coefficients in Eq.(1) are then $\zeta_\alpha = \Delta_\alpha/\Delta$ ³⁴, and the local chemical potential is thus $\mu^* = \frac{1}{3}\mu_L = -\frac{1}{6}V$.

Figure 2(b) depicts the relative change of observable $O = \chi^m$ or I_L^m , $[O_p(T_p, \mu^*) - (O_0 + \delta O_p)] / (O_0 + \delta O_p)$, versus the temperature of probe T_p . Clearly, $O_p(T_p, \mu^*)$ varies monotonically with the increasing T_p , and it crosses the reference value $(O_0 + \delta O_p)$ at a certain T_p , where the minimal (zero) perturbation condition is fulfilled, and we have $O_p(T_p, \mu^*) = O_0 + \delta O_p$. The perturbations of the two observables by the probe reduce to zero at roughly the same $T_p \simeq 0.28\Delta$. Therefore, from Eq.(3) we have $T^* = 0.28\Delta$ at $T = 0.133\Delta$.

In Fig. 2(a) we also compare T^* obtained by different protocols over a large range of T . It is shown that T^* determined by the minimal (zero) perturbation of χ^m

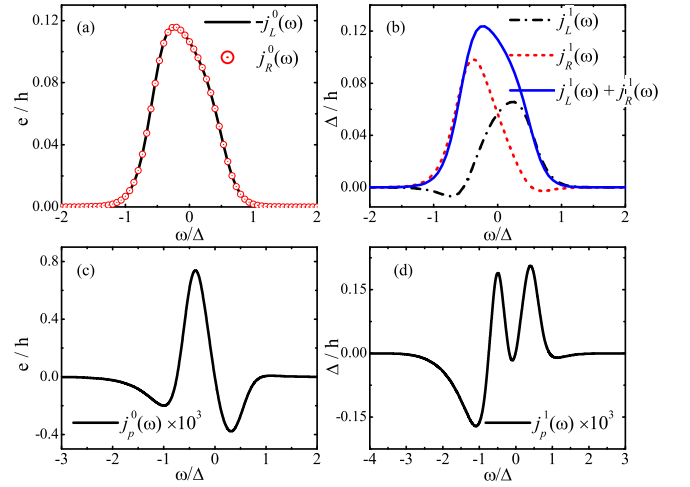


FIG. 3. Panels (a) and (b) depict the energy distribution of electric and heat currents flowing into α -lead ($\alpha = L, R$), respectively. Panels (c) and (d) plot the energy distribution of electric and heat currents flowing into the probe when the local equilibrium condition $I_p = J_p^H = 0$ is satisfied, respectively. The parameters adopted are (in units of Δ): $\epsilon_d = -2.67$, $U = 0$, $\Delta_L = 2\Delta_R = 100\Delta_p = 0.67$, $\mu_R = -\mu_L = 0.53$, $W = 40$, and $T_L = T_R = 0.133$.

and I_L^m agree remarkably well with each other (with a relative error less than 0.1%). They also agree closely and consistently with that obtained with the local equilibrium condition (with a relative error less than 4.5%). A closer look at both the electric and heat currents that flow between the probe and the system when the minimal perturbation is satisfied reveals that they are both close to zero (see Tables I and II), thus explaining the agreement between the two protocols. It is also found that, under a bias voltage, T^* is always higher than T , and their deviation increases as T decreases. In particular, T^* maintains a finite value (0.25Δ) even as $T \rightarrow 0$. This indicates that the local heating feature becomes more visible at a lower background T^1 .

Thermodynamically, the dot can be deemed as a reversed heat engine, and the leads act as heat baths as well as electron reservoirs. The internal energy of the dot is

$$\mathcal{U} = \mathcal{Q} + \mathcal{W} + \mu^* \langle \hat{n}_d \rangle, \quad (9)$$

with \mathcal{Q} and \mathcal{W} being the heat and work gained by the dot, respectively. Taking the time derivatives of both sides of Eq.(9) leads to

$$J_d^E = J_d^H + P + \mu^* \frac{d\langle \hat{n}_d \rangle}{dt}. \quad (10)$$

Here, J_d^E (J_d^H) is the energy (heat) current flowing into the dot, and P is the electric power. In a stationary state, \mathcal{U} is a constant, and thus $J_d^E = d\langle \hat{n}_d \rangle / dt = 0$. Therefore, $P = -J_d^H = \sum_\alpha J_\alpha^H$.

Figure 3(a) and (b) depict the energy distribution of bias driven electric and heat currents [$j_\alpha^0(\omega)$ and $j_\alpha^1(\omega)$]

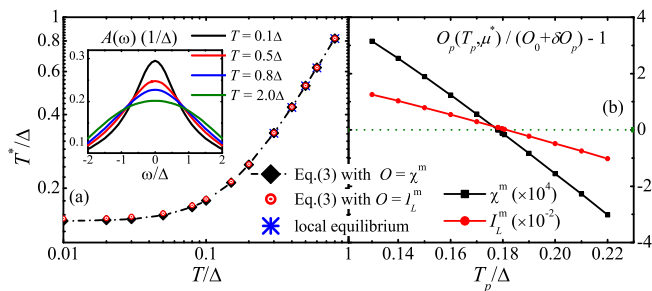


FIG. 4. (a) Local temperature T^* of an interacting QD determined by different protocols versus background T . The dashed line is a guide to eyes. The inset shows the Kondo spectral peak of the dot at various T . (b) Variation of system observables χ^m and I_L^m with T_p , at a background $T = 0.1\Delta$ lower than the Kondo temperature $T_K = 0.82\Delta$. The parameters adopted are (in units of Δ): $\epsilon_d = -1.2$, $U = 2.4$, $\Delta_L = \Delta_R = 0.5$, $\mu_R = -\mu_L = 0.25$, and $W = 5$.

in the noninteracting QD system studied in Fig. 2, respectively. In the absence of the probe, $j_L^0(\omega) = -j_R^0(\omega)$ holds for any ω , which ensures the conservation of electric current ($\sum_\alpha I_\alpha = 0$). In contrast, the heat currents flowing through left and right leads do not cancel out ($\sum_\alpha J_\alpha^H \neq 0$) – the dot behaves as a hot spot and dissipates heat into both leads.

To utilize the local equilibrium condition, the chemical potential μ_p and temperature T_p of the probe are tuned until the electric and heat currents flowing into the probe, $I_p = \int d\omega j_p^0(\omega)$ and $J_p^H = \int d\omega j_p^1(\omega)$, are both zero. Figure 3(c) and (d) display $j_p^0(\omega)$ and $j_p^1(\omega)$ when local equilibrium is reached ($I_p = J_p^H = 0$), respectively.

B. Local temperature of a Kondo QD

We now investigate interacting QDs under an anti-symmetric bias voltage. We choose to examine a half-filling dot with $U = -2\epsilon_d = 2.4\Delta$. It has been shown (through the temperature-dependent conductance) that this QD exhibits prominent Kondo features at $T < T_K$ ³⁸, with $T_K = 0.82\Delta$ being the characteristic Kondo temperature⁵². This is evident from the inset of Fig. 4(a) where the dot spectral function $A(\omega) = -\frac{1}{\pi}\text{Im}[\mathcal{G}^r(\omega)]$ is plotted for various background temperatures showing that the QD exhibits more prominent Kondo features as T lowers, as confirmed by the higher and sharper Kondo spectral peak centered at $\omega = \mu^*$. The chemical potentials of the leads are $\mu_R = -\mu_L = 0.25\Delta$. With the symmetric dot-lead couplings ($\Delta_L = \Delta_R$), the local chemical potential on the dot is $\mu^* = 0$ by Eq. (1).

Figure 4(a) compares T^* determined by different protocols. Limited by computational resources at our disposal, the HEOM calculations are done at $L = 4$ for the interacting QD⁵³. The results are considered to be highly accurate within the explored range of temperatures, since the computed conductance well reproduces

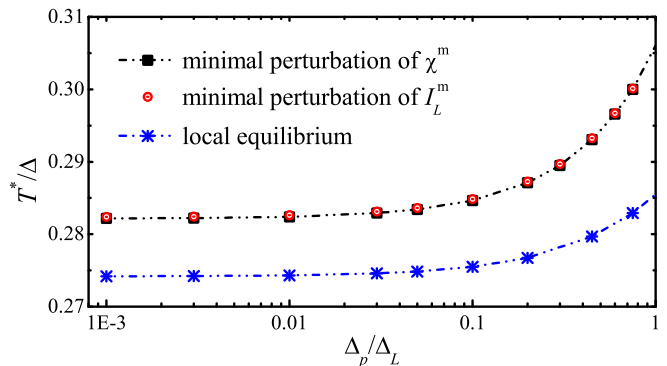


FIG. 5. Local temperature T^* of a noninteracting QD determined by different protocols versus the system-probe coupling strength Δ_p . The background temperature is fixed at $T = 0.133\Delta$. The parameters adopted are (in units of Δ): $\epsilon_d = -2.67$, $U = 0$, $\Delta_L = 2\Delta_R = 0.67$, $\mu_R = -\mu_L = 0.53$, and $W = 40$.

the Kondo scaling relation^{38,45}. As shown in Fig. 4(a), the local temperatures T^* determined by the minimal (zero) perturbation of χ^m and I_L^m agree remarkably well with each other (with a relative error less than 2%), as well as with the local equilibrium temperature (with a relative error less than 0.6%). This is again because the electric and heat currents flowing into the probe are both close to zero when the minimal perturbation is satisfied; see Tables I and II.

Similar to the noninteracting QD, the local temperature T^* on the interacting dot is always higher than the background T , and it approaches a finite value ($T^* \simeq 0.15\Delta$) as $T \rightarrow 0$. As clearly indicated by Fig. 4(b), both the relative changes of χ^m and I_L^m vary monotonically with T_p , while the latter has a much more sensitive temperature dependence. More importantly, the perturbations of both χ^m and I_L^m reduce to zero at almost the same T_p , which highlights again the generality of our operational definition.

C. The influence of probe-dot coupling strength Δ_p

We then investigate the influence of the coupling strength between the probe and the system. For numerical convenience we choose to examine the noninteracting QD explored in Fig. 2. Figure 5 shows T^* determined by using the minimal perturbation as well as the local equilibrium conditions. As the probe-dot coupling reduces to zero, all these temperatures approach a constant value as expected. More telling though is the fact that, even with a relatively large probe-dot coupling strength (comparable with the dot-lead couplings) the resulting T^* shows only a minor change of $\sim 7\%$, indicating again the robustness of the proposed protocol. We thus conclude that the measured local temperature depends rather insensitively on the probe-dot coupling Δ_p , which is favorable for experimental realizations.

| T/Δ | scaled electric current (e/h) | | | scaled heat current (Δ/h) | | | |
|------------|-----------------------------------|----------------|----------------|------------------------------------|------------------|------------------|--------------------------|
| | I_p/Δ_p | I_L/Δ_L | I_R/Δ_R | J_p^H/Δ_p | J_L^H/Δ_L | J_R^H/Δ_R | $(J_L^H + J_R^H)/\Delta$ |
| 0.133 | 2.9×10^{-3} | -0.37 | 0.74 | -9.8×10^{-3} | 0.16 | 0.47 | 0.26 |
| 0.667 | -5.5×10^{-2} | -0.54 | 1.08 | -0.17 | -0.25 | 1.65 | 0.39 |

TABLE I. Electric and heat currents flowing into leads coupled to a noninteracting QD when the minimal (zero) perturbation condition is satisfied. The parameters adopted are (in units of Δ): $\epsilon_d = -2.67$, $U = 0$, $\Delta_L = 2\Delta_R = 100\Delta_p = 0.67$, $\mu_R = -\mu_L = 0.53$, and $W = 40$.

| T/Δ | scaled electric current (e/h) | | | scaled heat current (Δ/h) | | | |
|------------|-----------------------------------|----------------|----------------|------------------------------------|------------------|------------------|--------------------------|
| | I_p/Δ_p | I_L/Δ_L | I_R/Δ_R | J_p^H/Δ_p | J_L^H/Δ_L | J_R^H/Δ_R | $(J_L^H + J_R^H)/\Delta$ |
| 0.4 | -1.3×10^{-9} | -1.32 | 1.32 | -6.9×10^{-3} | 1.33 | 1.33 | 2.66 |
| 0.8 | -4.9×10^{-11} | -1.01 | 1.01 | -3.9×10^{-3} | 1.02 | 1.02 | 2.04 |

TABLE II. Electric and heat currents flowing into leads coupled to an interacting QD when the minimal (zero) perturbation condition is satisfied. The parameters adopted are (in units of Δ): $\epsilon_d = -1.2$, $U = 2.4$, $\Delta_L = \Delta_R = 100\Delta_p = 0.5$, $\mu_R = -\mu_L = 0.25$, and $W = 5$.

As demonstrated clearly in Sec. III A and III B, the local temperatures measured by using the minimal perturbation condition agree closely and consistently with those determined by the local equilibrium condition. This is because both the electric and heat currents flowing into the probe are close to zero when the minimal perturbation condition is satisfied. Tables I and II verify that when the minimal perturbation is reached the values of both I_p and J_p^H are indeed negligibly small for the noninteracting and interacting QDs investigated in Sec. III, respectively. It is clearly seen from the tables that, even after being scaled by the small dot-probe coupling strength Δ_p , the electric and heat currents flowing through the probe are still much smaller than the currents flowing into the left and right leads.

D. Local temperature of a QD subjected to a thermal gradient

Finally, we demonstrate that the proposed operational definition of local temperature, Eqs. (1)–(4), is also applicable to QDs subjected to an applied thermal gradient, *i.e.*, when $\Delta T = T_R - T_L \neq 0$. Note that for this to be true, the bias voltage must be zero ($\mu_R = \mu_L$), and thus the electric current is driven only by the thermal gradient ΔT .

In the absence of bias voltage, Eq. (1) becomes trivial since $\mu^* = \mu_L = \mu_R$. Therefore, the chemical potential of the probe is fixed at $\mu_p = \mu_L = \mu_R$, and we only need to tune T_p ³¹. When $T_p = T^*$, the electric current flowing into the probe vanishes. We thus have

$$(T^* - T_L)L_{Lp}^T = (T_R - T^*)L_{Rp}^T. \quad (11)$$

Here, $L_{\alpha p}^T$ is the thermoelectric transmission coefficient between lead- α and probe. Through an analysis similar to that in Appendix, one arrives at a simple expression

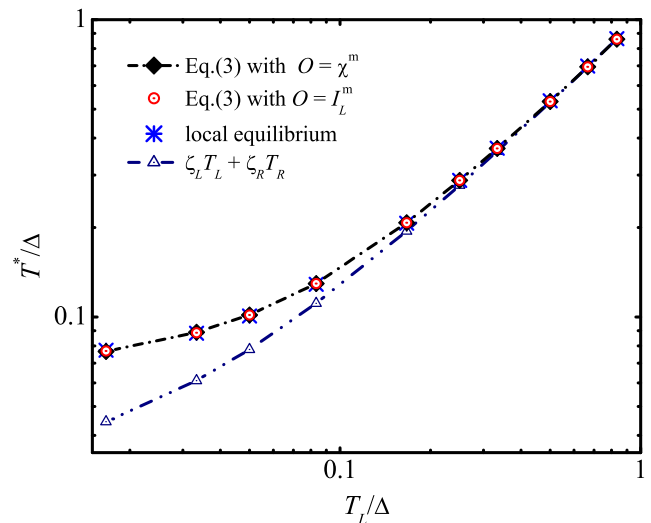


FIG. 6. T^* of a noninteracting QD versus the temperature of left lead T_L . The parameters adopted are (in units of Δ): $\epsilon_d = -3.33$, $U = 0$, $\Delta_L = 5\Delta_R = 0.83$, $\mu_R = \mu_L = 0$, $\Delta T = T_R - T_L = 0.17$, and $W = 50$.

of T^* as

$$T^* = \zeta_L T_L + \zeta_R T_R. \quad (12)$$

Here, the weight coefficients ζ_L and ζ_R are also given by the last equality of Eq. (2). However, Eq. (12) turns out to be a rather crude estimate of T^* , as shown in Fig. 6. The accurate measurement of T^* is achieved by using Eqs. (3)–(4).

For instance, consider a general case such that dot-lead couplings are asymmetric with $\Delta_L = 5\Delta_R$. The weight coefficients $\zeta_L = \frac{5}{6}$ and $\zeta_R = \frac{1}{6}$ agree well with the “measured” values of $\zeta_L = 0.8333$ and $\zeta_R = 0.1667$ by Eq. (2). Figure 6 compares T^* obtained by different approaches. Clearly, T^* determined by minimal (zero)

perturbation of χ^m and I_L^m agree remarkably well with the prediction of local equilibrium condition.

It should be pointed out that, when a bias voltage and thermal gradient are both present, the electric current through a certain lead is driven by both V and ΔT . In such a case, the simple relation of Eq. (A.1) no longer holds. Therefore, the proposed operational definition is not applicable to the scenario in which both V and ΔT are nonzero.

IV. CONCLUDING REMARKS

In conclusion, we have proposed an operational definition of local temperature for bias-driven QDs using a “minimal perturbation condition”, as represented by Eqs. (1)–(4). The same definition is also applicable to QDs subjected to external thermal gradients. The operational definition applies equally well to systems ranging from noninteracting to Kondo-correlated regimes. Since this definition does not require measurements of heat currents, its experimental realization is straightforward. The “minimal perturbation condition” thus provides a useful practical means to examine local electron excitations in a nonequilibrium process, in which local heating plays an important role.

The local temperature is a characterization of local statistical excitations in the nanoscale systems. When the QDs are tuned to different regimes, such as Kondo regime, Coulomb blockade regime and mixed-valence regime, different electronic structures may lead to different local temperatures, which remain to be further investigated. Such studies are currently underway.

V. ACKNOWLEDGMENTS

The support from the National Natural Science Foundation of China (Grants No. 21233007 and No. 21322305), and the Strategic Priority Research Program (B) of the Chinese Academy of Sciences (XDB01020000) is gratefully appreciated. MD acknowledges support from DOE under Grant No. DE-FG02-05ER46204.

Appendix: Remarks on the weight coefficients ζ_L and ζ_R

Suppose $T_L = T_R$. The electric current between left and right leads is driven only by the applied bias voltage (difference in chemical potentials). With the chemical potential of probe μ_p aligned with the dot local chemical potential μ^* , the net electric current flowing into the probe is exactly zero. This is because the electric currents coming from the left and right leads cancel out exactly:

$$(\mu^* - \mu_L)G_{Lp} = (\mu_R - \mu^*)G_{Rp}. \quad (\text{A.1})$$

Here, $G_{\alpha p}$ ($\alpha = L, R$) is the electron conductance between lead- α and the probe. Rearranging Eq. (A.1), we have

$$\mu^* = \frac{G_{Rp}}{G_{Lp} + G_{Rp}}\mu_R + \frac{G_{Lp}}{G_{Lp} + G_{Rp}}\mu_L. \quad (\text{A.2})$$

By setting $\mu_p = \mu_\alpha$ and $T_p = T_\alpha$, the probe can be deemed as a part of lead- α . Therefore, the electric current flowing through the probe I_p amounts to

$$I_p(T_L, \mu_L) = G_{Rp}(\mu_L - \mu_R), \quad (\text{A.3})$$

$$I_p(T_R, \mu_R) = G_{Lp}(\mu_R - \mu_L), \quad (\text{A.4})$$

and hence $\frac{G_{Rp}}{G_{Lp}} = -\frac{I_p(T_L, \mu_L)}{I_p(T_R, \mu_R)}$. Here, the two currents have opposite signs. By comparing Eq. (A.2) and Eq. (1), it is clear that the weight coefficient ζ_α should be proportional to the two-terminal conductance $G_{\alpha p}$, as follows

$$\zeta_\alpha = \frac{G_{\alpha p}}{G_{Lp} + G_{Rp}} = 1 - \left| \frac{I_p(T_\alpha, \mu_\alpha)}{I_p(T_L, \mu_L) - I_p(T_R, \mu_R)} \right|. \quad (\text{A.5})$$

Here, we have assumed that $G_{\alpha p}$ does not change significantly with μ_p and T_p . Obviously, the weight coefficients should normalize to unity, $\zeta_L + \zeta_R = 1$.

For the single-impurity Anderson model investigated in this paper, if all leads have the same form of hybridization function, *i.e.*, $\Delta_\alpha(\omega) = \Delta_\alpha \eta(\omega)$ ($\alpha = L, R$ and p), we have

$$I_p(T_L, \mu_L) = \left(\frac{\Delta_p}{\Delta_L + \Delta_p} \right) \cdot \left(-\frac{2}{\pi} \right) \frac{(\Delta_L + \Delta_p)\Delta_R}{\Delta_L + \Delta_R + \Delta_p} \times \int d\omega [f_{\beta_L}(\omega - \mu_L) - f_{\beta_R}(\omega - \mu_R)] \text{Im}[\mathcal{G}^r(\omega)], \quad (\text{A.6})$$

$$I_p(T_R, \mu_R) = \left(\frac{\Delta_p}{\Delta_R + \Delta_p} \right) \cdot \left(-\frac{2}{\pi} \right) \frac{(\Delta_R + \Delta_p)\Delta_L}{\Delta_L + \Delta_R + \Delta_p} \times \int d\omega [f_{\beta_R}(\omega - \mu_R) - f_{\beta_L}(\omega - \mu_L)] \text{Im}[\mathcal{G}^r(\omega)], \quad (\text{A.7})$$

with $\beta_\alpha = 1/T_\alpha$. Here, the probe is deemed as part of lead- α , and the SIAM amounts to a two-terminal model. Therefore, Eq. (9) of Ref. 47 can be used. Equations (A.6) and (A.7) immediately lead to the relation of

$$\frac{I_p(T_L, \mu_L)}{I_p(T_R, \mu_R)} = -\frac{\Delta_R}{\Delta_L}. \quad (\text{A.8})$$

Equation (A.8) thus offers a practical means of determining the ratio Δ_R/Δ_L in experiments. Consequently, by combining Eqs. (A.5) and (A.8), we have

$$\zeta_\alpha = \frac{\Delta_\alpha}{\Delta_L + \Delta_R} \quad (\text{A.9})$$

for $\alpha = L$ or R .

| ζ_L | Fig. 2 noninteracting QD | Fig. 4 Kondo-correlated QD |
|-----------|-----------------------------|-------------------------------|
| Eq. (A.5) | 0.6666 | 0.5000 |
| Eq. (A.9) | $\frac{2}{3}$ | $\frac{1}{2}$ |

TABLE III. The weight coefficient ζ_L for the QDs studied in Figs. 2 and 4. The numbers are obtained via Eqs. (A.5) and (A.9), respectively.

Since the electric current flowing into the probe I_p can be measured straightforwardly, the weight coefficients $\{\zeta_\alpha\}$ are obtained readily from Eq. (A.5). Table III lists the weight coefficient ζ_L for the QDs studied in Figs. 2 and 4. The numbers obtained via Eq. (A.5) and (A.9) agree precisely with each other.

* xz58@ustc.edu.cn

† diventra@physics.ucsd.edu

- 1 M. Di Ventra, *Electrical Transport in Nanoscale Systems*, Cambridge University Press, Cambridge, 2008.
- 2 H.-L. Engquist and P. W. Anderson, Phys. Rev. B **24**, 1151 (1981).
- 3 M. Galperin, A. Nitzan, and M. A. Ratner, Phys. Rev. B **75**, 155312 (2007).
- 4 M. Galperin, M. A. Ratner, and A. Nitzan, J. Phys.: Condens. Matter **19**, 103201 (2007).
- 5 A. Caso, L. Arrachea, and G. S. Lozano, Phys. Rev. B **81**, 041301 (2010).
- 6 A. Caso, L. Arrachea, and G. S. Lozano, Phys. Rev. B **83**, 165419 (2011).
- 7 D. Sánchez and L. Serra, Phys. Rev. B **84**, 201307 (2011).
- 8 P. A. Jacquet and C.-A. Pillet, Phys. Rev. B **85**, 125120 (2012).
- 9 J. P. Bergfield, S. M. Story, R. C. S. , and C. A. Stafford, ACS Nano **7**, 4429 (2013).
- 10 J. P. Bergfield, M. A. Ratner, C. A. Stafford, and M. Di Ventra, arXiv:1305.6602 (2013).
- 11 J. Meair, J. P. Bergfield, C. A. Stafford, and P. Jacquod, Phys. Rev. B **90**, 035407 (2014).
- 12 Y. Dubi and M. Di Ventra, Rev. Mod. Phys. **83**, 131 (2011).
- 13 J. P. Pekola et al., Phys. Rev. Lett. **92**, 056804 (2004).
- 14 M. Di Ventra and Y. Dubi, Europhys. Lett. **85**, 40004 (2009).
- 15 A. Caso, L. Arrachea, and G. S. Lozano, Eur. Phys. Jour. B **85**, 266 (2012).
- 16 Z. Huang, B. Xu, Y. Chen, M. Di Ventra, and N. Tao, Nano Lett. **6**, 1240 (2006).
- 17 M. Tsutsui, M. Taniguchi, and T. Kawai, Nano Lett. **8**, 3293 (2008).
- 18 M. Tsutsui, T. Morikawa, A. Arima, and M. Taniguchi, Sci. Rep. **3**, 3326 (2013).
- 19 Z. Huang et al., Nat. Nanotechnol. **2**, 698 (2007).
- 20 R. Chen, P. J. Wheeler, M. Di Ventra, and D. Natelson, Sci. Rep. **4**, 4221 (2013).
- 21 Z. Ioffe et al., Nat. Nanotechnol. **3**, 727 (2008).
- 22 D. R. Ward, D. A. Corley, J. M. Tour, and D. Natelson, Nat. Nanotechnol. **6**, 33 (2011).
- 23 S. Sadat, A. Tan, Y. J. Chua, and P. Reddy, Nano Lett. **10**, 2613 (2010).
- 24 K. L. Grosse, M.-H. Bae, F. Lian, E. Pop, and W. P. King, Nat. Nanotechnol. **6**, 287 (2011).
- 25 K. Kim, J. Chung, G. Hwang, O. Kwon, and J. S. Lee, ACS Nano **5**, 8700 (2011).
- 26 F. Menges, H. Riel, A. Stemmer, and B. Gotsmann, Nano Lett. **12**, 596 (2012).

- 27 K. Kim, W. Jeong, W. Lee, and P. Reddy, ACS Nano **6**, 4248 (2012).
- 28 F. Menges, H. Riel, A. Stemmer, C. Dimitrakopoulos, and B. Gotsmann, Phys. Rev. Lett. **111**, 205901 (2013).
- 29 Y. Kim, W. Jeong, K. Kim, W. Lee, and P. Reddy, Nat. Nanotechnol. **9**, 881 (2014).
- 30 M. Mecklenburg et al., Science **347**, 629 (2015).
- 31 Y. Dubi and M. Di Ventra, Nano Lett. **9**, 97 (2009).
- 32 Y. Dubi and M. Di Ventra, Phys. Rev. B **79**, 115415 (2009).
- 33 We exclude the scenario that bias voltage and thermal gradient are both present, which is beyond the applicability of the protocol proposed in this work, see the last paragraph of Sec. III D for more details.
- 34 See Appendix for more details on the derivation and computation of the weight coefficients ζ_L and ζ_R .
- 35 P. W. Anderson, Phys. Rev. **124**, 41 (1961).
- 36 Y. Meir, N. S. Wingreen, and P. A. Lee, Phys. Rev. Lett. **70**, 2601 (1993).
- 37 J. S. Jin, X. Zheng, and Y. J. Yan, J. Chem. Phys. **128**, 234703 (2008).
- 38 Z. H. Li et al., Phys. Rev. Lett. **109**, 266403 (2012).
- 39 X. Zheng, J. S. Jin, and Y. J. Yan, New J. Phys. **10**, 093016 (2008).
- 40 S. K. Wang, X. Zheng, J. S. Jin, and Y. J. Yan, Phys. Rev. B **88**, 035129 (2013).
- 41 X. Zheng, J. S. Jin, S. Welack, M. Luo, and Y. J. Yan, J. Chem. Phys. **130**, 164708 (2009).
- 42 X. Zheng, Y. J. Yan, and M. Di Ventra, Phys. Rev. Lett. **111**, 086601 (2013).
- 43 D. Hou et al., Phys. Rev. B **90**, 045141 (2014).
- 44 Y. Wang, X. Zheng, B. Li, and J. Yang, J. Chem. Phys. **141**, 084713 (2014).
- 45 L. Ye et al., Phys. Rev. B **90**, 165116 (2014).
- 46 X. Zheng et al., Prog. Chem. **24**, 1129 (2012).
- 47 Y. Meir and N. S. Wingreen, Phys. Rev. Lett. **68**, 2512 (1992).
- 48 B. Dong and X. L. Lei, J. Phys.: Condens. Matter **14**, 11747 (2002).
- 49 J. P. Bergfield and C. A. Stafford, Phys. Rev. B **79**, 245125 (2009).
- 50 A. A. Aligia, Phys. Rev. B **89**, 125405 (2014).
- 51 P. Mani, N. Nakpathomkun, E. Hoffmann, and H. Linke, Nano Lett. **11**, 4679 (2011).
- 52 A. C. Hewson, *The Kondo Problem to Heavy Fermions*, Cambridge University Press, Cambridge, 1993.
- 53 For interacting QDs a higher truncation level L is needed to converge the heat current J_α^H than to converge the reduced density matrix ρ . Therefore, it is computationally much more demanding to determine T^* by using the lo-

cal equilibrium condition. Limited by computational resources, the local equilibrium condition can only be applied

at background temperatures $T > 0.3\Delta$.